

BASIC SCIENCES

Injury Length and Arteriole Constriction Shape Clot Growth and Blood-Flow Acceleration in a Mouse Model of Thrombosis

Alexander Y. Mitrophanov¹, Glenn Merrill-Skoloff, Steven P. Grover, Vijay Govindarajan, Arun Kolanjiyil, Daniel S. Hariprasad, Ginu Unnikrishnan, Robert Flaumenhaft, Jaques Reifman¹

OBJECTIVE: Quantitative relationships between the extent of injury and thrombus formation in vivo are not well understood. Moreover, it has not been investigated how increased injury severity translates to blood-flow modulation. Here, we investigated interconnections between injury length, clot growth, and blood flow in a mouse model of laser-induced thrombosis.

APPROACH AND RESULTS: Using intravital microscopy, we analyzed 59 clotting events collected from the cremaster arteriole of 14 adult mice. We regarded injury length as a measure of injury severity. The injury caused transient constriction upstream and downstream of the injury site resulting in a 50% reduction in arteriole diameter. The amount of platelet accumulation and fibrin formation did not depend on arteriole diameter or deformation but displayed an exponentially increasing dependence on injury length. The height of the platelet clot depended linearly on injury length and the arteriole diameter. Upstream arteriolar constriction correlated with delayed upstream velocity increase, which, in turn, determined downstream velocity. Before clot formation, flow velocity positively correlated with the arteriole diameter. After the onset of thrombus growth, flow velocity at the injury site negatively correlated with the arteriole diameter and with the size of the above-clot lumen.

CONCLUSIONS: Injury severity increased platelet accumulation and fibrin formation in a persistently steep fashion and, together with arteriole diameter, defined clot height. Arterial constriction and clot formation were characterized by a dynamic change in the blood flow, associated with increased flow velocity.

GRAPHIC ABSTRACT: A [graphic abstract](#) is available for this article.

Key Words: arteriole ■ constriction ■ fibrin ■ intravital microscopy ■ mice

The formation of a clot inside a blood vessel—thrombosis—links the molecular and cellular factors that cause it with its anticipated fluid-dynamical final outcome: the change of blood flow through the stenosed vessel.¹ Despite the existing detailed knowledge about the molecular and cellular determinants of thrombus formation, the complex interplay between biological and physical factors involved is still insufficiently understood.^{2,3} Improved understanding of the relationships between the degree of thrombus growth and the magnitude of

the resulting changes in the blood flow may improve our ability to control the flow by modulating clot growth via therapeutic intervention.

Microfluidic experiments with manufactured thrombogenic surfaces generally indicate that clot growth under flow is enhanced by increasing tissue factor abundance, and also by increasing thrombogenic-surface length within certain limits.^{4–7} This enhancement can display threshold-like behavior^{6,7}; yet, thresholds are not always observed.^{4,5,8} Moreover, the effect of

Correspondence to: Alexander Y. Mitrophanov, PhD, Department of Defense Biotechnology High Performance Computing Software Applications Institute, Telemedicine and Advanced Technology Research Center, US Army Medical Research and Development Command, ATTN: FCMR-TT, 504 Scott St, Ft. Detrick, MD, Email alex@bhsai.org; or Jaques Reifman, PhD, Department of Defense Biotechnology High Performance Computing Software Applications Institute, Telemedicine and Advanced Technology Research Center, US Army Medical Research and Development Command, ATTN: FCMR-TT, 504 Scott St, Ft. Detrick, MD, Email jaques.reifman.civ@mail.mil

The Data Supplement is available with this article at <https://www.ahajournals.org/doi/suppl/10.1161/ATVBAHA.120.314786>.

For Sources of Funding and Disclosures, see page 2125.

© 2020 American Heart Association, Inc.

Arterioscler Thromb Vasc Biol is available at www.ahajournals.org/journal/atvb

Nonstandard Abbreviations and Acronyms

RBC	red blood cell
------------	----------------

thrombogenic-surface length on platelet-clot height may not always be clearly pronounced,⁵ suggesting that bulk clot size and the clot's ability to obstruct the channel may be regulated differently. Tissue factor is regarded as the main physiological activator of clot formation. In static (no flow) *in vitro* assays, increased tissue factor level is expected to accelerate the formation of thrombin and, therefore, fibrin—the essential biochemical components of the clot.^{9,10} The other key process is platelet accumulation, which can be interlinked with fibrin formation.^{11,12} The influence of these (and possibly many other) factors on clot growth initiation and propagation are challenging to disentangle *in vivo*.

Availability of this information raises the question of how the severity of an injury—which can expose TF¹³ and trigger platelet accumulation¹¹—affects clot formation *in vivo*, and the existing experimental evidence is limited. Thrombus formation in the rabbit femoral artery displayed a possible correlation with injury length upon post-stenotic endothelial damage.¹⁴ In a laser-injury mouse thrombosis model, injury severity (depth) correlated with its length; the deep injury resulted in a considerably increased thrombus area compared with the superficial injury.^{15,16} A recent study combined confocal-microscopy data on 10 clots with a computational clot-volume reconstruction algorithm to quantify the dependence of platelet-clot volume on injury length and blood-vessel diameter; the dependence was found to be nonlinear.¹⁷ Yet, the effects of injury severity on the amount of distinct clot components, the rate of their deposition, and ultimately on the ability of a growing clot to obstruct the blood vessel remain insufficiently characterized. Moreover, the current views regarding the effects of clot formation on blood-flow velocity *in vivo* seem to show opposing patterns. On the one hand, clot formation inside a blood vessel—similarly to a stenosis or ligation—is expected to reduce the velocity of the flow near it under realistic conditions *in vitro*^{18,19} and *in vivo*,^{20–23} because the increased resistance diverts the flow elsewhere.^{24,25} On the other hand, different simulation approaches to thrombus formation suggest that, as the clot continues to grow, the velocity in its vicinity will continue to increase,^{17,26,27} which may contribute to platelet activation *in vivo*.^{1,28}

Here, we attempted to address these knowledge gaps using intravital-microscopy data on laser-induced thrombus formation in the mouse cremaster arteriole. Our approach was based on the analysis of three types of intravascular-microscopy data: (1) injury-length and arteriole-diameter measurements from brightfield images, (2) platelet and fibrin fluorescence kinetics at the injury

Highlights

- Laser-induced injury to mouse cremaster arteriole was followed by a rapid, yet transient, constriction up to 2-fold upstream and downstream of the injury site.
- Bulk platelet and fibrin accumulation exponentially increased with injury length and was uncorrelated with arteriole deformation.
- Absolute and relative platelet-clot height were increasing linear functions of injury length.
- In the first seconds post-injury, flow velocity at the injury site positively correlated with the arteriole diameter.
- Blood-flow velocity upstream and downstream of the injury site increased because of arteriole constriction, and the velocity at the injury site during clot growth negatively correlated with the arteriole diameter and the above-clot lumen size.

site, and (3) flow-velocity estimates using fluorescently labeled red blood cells (RBCs; Figure 1A), which is a novel application of this approach in the context of clot formation. We hypothesized a steep functional dependence of platelet and fibrin deposition on injury size (specifically, on its length), which would consistently translate to increased clot height, indicative of the clot's capacity for flow obstruction. Moreover, we hypothesized that, in the presence of a clot or a vessel constriction, the blood-flow velocity can indeed be increased, which may differ from the typical pattern observed for unperturbed blood vessels in a microvascular bed.

MATERIALS AND METHODS

The data that support the findings of this study are available from the corresponding authors upon reasonable request.

The Mouse Data Set

This study was approved by the Beth Israel Deaconess Medical Center Institutional Animal Care and Use Committee (Boston, MA) and the US Army Animal Care and Use Review Office (Ft. Detrick, MD). The experiments and raw image-data processing were performed at Beth Israel Deaconess Medical Center, whereas the subsequent computational and statistical analysis was carried out at the DoD Biotechnology High Performance Computing Software Applications Institute (BHSAI).

We used wild-type mice (see the Major Resources Table in the [Data Supplement](#)) to collect clot-growth and flow-velocity data, cremaster-arteriole diameter data, and injury-length measurements on individual thrombi (clotting events) (Figure 1A). Although there are other preparations and surgical approaches for studying thrombus formation via intravital microscopy, the cremaster muscle in the male anatomy provides for a particularly clean preparation that leaves the arteriole free of excessive connective tissue. For these advantages, we were restricted to using male mice.

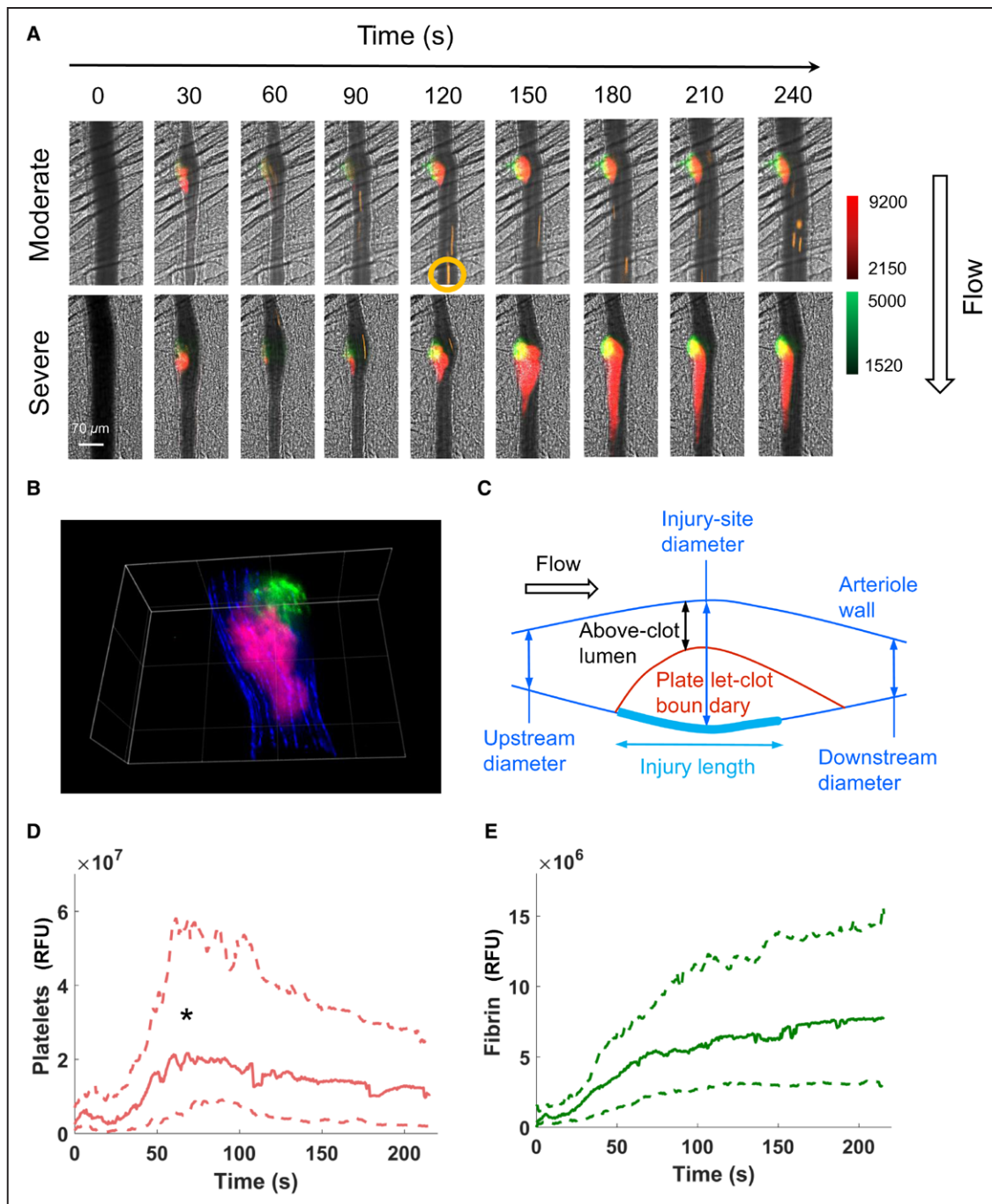


Figure 1. Thrombus growth, vessel deformation, and red blood cell (RBC) flow in the mouse cremaster arteriole.

A, time dependence of thrombus growth and arteriole deformation in combined widefield (fluorescence) and brightfield images. The top and bottom panels show a less occlusive and a more occlusive representative clots, respectively. Red, platelets; green, fibrin; gold streaks (such as the one indicated by a circle in the top panel), RBCs. The numbers on top indicate time in seconds. The arrow on the right shows blood-flow direction. The vertical red and green bars on the right show the color-intensity scales. The white horizontal bar in the bottom left corner marks a 70- μ m distance. **B**, a representative clot in three dimensions. Magenta, platelets; green, fibrin; blue, endothelial cells. The distance between the thin lines is 50 μ m. The endothelium surrounds the clot. Fibrin formation occurs in close apposition to the endothelium and typically at the site of laser injury. Platelets accumulate in the lumen of the vessel. In this representative image, the clot is subocclusive because the platelets do not occupy the entire diameter of the vessel. **C**, Schematic of essential characteristics of an individual clotting event analyzed in the present study, corresponding to 2-dimensional widefield and brightfield views. **D** and **E**, Bulk accumulation kinetics for platelets and fibrin, respectively (N=59). Solid and dashed lines correspond to the medians and interquartile distances, respectively. For platelets, the \approx 2-fold median decay was significant (peak median [marked with the asterisk] vs end-point median [at 215.5 s], $P=1.6 \times 10^{-5}$). RFU indicates raw fluorescence unit.

We excluded some of the clots for different reasons. A list of clot-exclusion criteria, defined before study initiation, is given in the [Data Supplement](#). We additionally excluded eight thrombi for which the collected data were insufficient for flow-velocity estimation. We performed full analysis on 59 thrombi from 14 mice. To evaluate the spatial relationships between the clot and endothelium, we additionally collected confocal-microscopy data on a separate group of 48 cremaster-arteriole clots from 7 more mice (Figure 1B).

As preoperative anesthetic, we used a cocktail of 125 mg/kg ketamine with 12.5 mg/kg xylazine injected intraperitoneally one time in 300 μ L sterile saline. As intraoperative anesthetic, we used pentobarbital (50 mg/kg) injected intravenously via a jugular vein catheter as needed (\approx every 30 minutes) in 30 μ L sterile saline. These procedures were terminal, and euthanasia was achieved by a one-time bolus of intravenous injection of pentobarbital in excess of 200 mg/kg followed by cervical dislocation.

Cremaster-Arteriole Model of Thrombosis

We performed the laser-injury thrombosis model as previously described.²⁹ Briefly, we injured cremaster arterioles using 24 pulses (in a two-by-two closely spaced array, repeated 6 \times) from a dye-tuned nitrogen pulse laser (Andor; Belfast, United Kingdom) configured to produce nanosecond laser-light pulses at 440 nm. We aimed the pulses at or near the arteriole vessel wall, which produced a distortion discernable by eye in brightfield images. We measured platelet and fibrin accumulation following injury using a 40 \times , numerical aperture 1.0 objective lens (Olympus; Tokyo, Japan). We used SlideBook 6 (Intelligent Imaging Innovations, Inc; Denver, CO) to handle hardware control, image capture, and much of the image analysis. Ultimately, we digitized the image data and subjected them to computational analyses.

Intravital Microscopy

The widefield intravital fluorescence microscopy system has previously been described.¹³ Modifications of the imaging system that were used in the present study include an Orca-Flash 4.0 sCMOS camera (Hamamatsu; Hamamatsu City, Japan) to capture digital video images, a LED-based SpectraX light engine (Lumencor; Beaverton, OR) using 6 solid-state light sources, and a LED-based white-light source (Prior Scientific; Rockland, MA). See [Data Supplement](#) for further details.

We used the SlideBook 6 and ImageJ (National Institutes of Health; Bethesda, MD) software to measure injury lengths and arteriole diameters directly from the brightfield images acquired simultaneously with the widefield fluorescence images. We quantified injury length by measuring the distance along the long axis of the ovoid-shaped distortion produced in the arteriole wall at the injury site following the ablative event. We measured the arteriole diameters at the injury site, as well as 130 μ m upstream and downstream of it. We chose to focus on locations closer to the thrombus to investigate possible interference. We used the widefield images to measure the height of platelet clots at the time of their maximum extent.

RBC Labeling and Blood-Flow Velocity Measurement

We measured RBC velocity approximating the centerline flow velocity in the regions of the arteriole upstream and

downstream from the injury site, as well as in the region over it. The velocity was determined by introducing three to four million exogenous RBCs via a jugular-vein catheter before the first injury in a series. We isolated these RBCs from donor mice and labelled them using the Cell-Tracker Orange CMTMR dye (Thermo-Fisher Scientific; Waltham, MA). After image capture, we measured the distance traveled per unit time for up to 400 individual RBCs over the entire time course of the experimental observation using ObjectJ, an ImageJ plug-in. To convert the raw data (velocity values for distinct red blood cell markers) to velocity time courses for each clotting event, we used custom-written scripts in MATLAB R2017b (MathWorks; Natick, MA).

Further methodological details regarding our experimental procedures are provided in the [Data Supplement](#).

Statistical Analysis

We performed all statistical analyses in MATLAB R2017b (with the Statistics and Machine Learning Toolbox) using custom-written scripts. In all computational procedures, we analyzed the data from individual clotting events (N=59), which we pooled from 14 mice. The pooling was based on our analysis of data variables (such as the area under the curve for the platelet and fibrin bulk-fluorescence time courses) from individual mice using the Kruskal-Wallis test, which did not identify statistically significant differences between the 14 mice. We regarded $P < 0.05$ as statistically significant.

We reported the data as the mean \pm 1 SD (referred for normally distributed quantities) or as the median and interquartile range.³⁰ We used the Jarque-Bera test to assess normality.³¹ For pairwise comparisons of means and medians, we used the paired *t*-test and Wilcoxon signed rank test, respectively.³⁰

We used stepwise linear regression to analyze the dependence of the (natural) logarithms of platelet and fibrin bulk-fluorescence parameters on 3 predictor variables: injury length and the maximum upstream- and downstream-diameter fold changes.³² For each individual clotting event, we divided the upstream-diameter values measured at times greater than zero by the upstream diameter at time zero; if the result was < 1 , then the reciprocal value was taken. (Time zero corresponded to the frame immediately following the ablation event, and was the same for platelet and fibrin accumulation as it was for RBC velocity measurements.) Then, we defined maximum fold change as the largest of these values. We calculated maximum downstream-diameter fold change analogously.

In the stepwise regression, we rescaled the predictor variables using the min-max scaling, which restricted them to varying in the $(-1, 1)$ range.³² The initial regression equation included all one-variable terms and also 2- and 3-way interaction terms (ie, products of variables). We then fit the initial model to the data and obtained a reduced regression equation with fewer terms. The *P*-value thresholds for automatic term removal and addition were 0.05 and 0.01, respectively (MATLAB requires them to be different). In other cases of linear regression analysis, we used bivariate or univariate regression without model reduction. We performed nonlinear univariate regression analysis by fitting the equation $y = a \times \exp(b \times x)$. We assessed the strength of nonlinear regression using its coefficient of determination (R^2); for linear regression, R^2 was supplemented by a *P*-value testing the null hypothesis of a flat regression function. To assess the strength of monotonic (not

necessarily linear) associations between 2 data samples, we used Spearman correlation coefficient (ρ) with a P -value testing the null hypothesis of $\rho=0$.

One particular case of univariate linear regression concerned the relationship between cremaster-arteriole diameter (or the above-clot lumen, Figure 1C) and flow velocity. The rationale for such a linear relationship is provided in the [Data Supplement](#).

RESULTS

Injuries of Variable Length Are Followed by Clot Growth, Dynamic Arteriole Deformations, and Flow-Velocity Change

The bulk-fluorescence time courses were characterized by a peak, sometimes preceded by a smaller peak, for platelets and by largely monotonic increase, sometimes reaching a plateau, for fibrin. This was manifested in the median behavior (Figure 1D and 1E) and also in the time courses for individual clotting events. Injury length demonstrated considerable variability (mean \pm 1 SD, 75.7 \pm 22.7 μ m), which was a key observation motivating our data-driven approach. Notably, the cremaster-arteriole diameter (mean \pm 1 SD, 52.1 \pm 8.2 μ m) was smaller ($P=1.6\times 10^{-10}$) than injury length, suggesting an elliptical injury shape with the ellipse's major axis aligned with the arteriole axis. This was consistent with both our widefield and our confocal data showing prolonged platelet-clot shapes, which were additionally impacted by platelet wash-off (Figure 1A and 1B). These data consistently showed clot morphology where the platelet-accumulation region defined the overall clot boundary, which justified our focus on platelet clot height (Figure 1C). Of the 59 clots analyzed, 16 reached maximum possible (100%) relative height (with respect to the arteriole diameter)—that is, their above-clot lumen (defined in Figure 1C) was zero.

We detected dynamic changes in the cremaster-arteriole diameter that occurred immediately following injury. The arteriole quickly constricted (the measured reduction in the average diameter was most pronounced at 15 seconds) and then slowly dilated toward its initial diameter (Figure 2A through 2C). As was evident from the brightfield images, the constriction typically affected arteriole segments stretching for a certain length up- and downstream of the injury site (Figure 1A). The average diameter decreased up to 1.14-fold at the injury site, and up to \approx 2-fold 130 μ m upstream and downstream of the injury (Figure 2A through 2C). Whereas there was an apparent causal relationship between injury induction and vessel constriction, the maximum diameter fold change and injury length were uncorrelated (Figure I in the [Data Supplement](#)). These results allowed us to regard injury length and the extent of arteriole constriction as independent variables in our subsequent statistical analyses.

Our velocity measurements demonstrated temporal velocity changes at the injury site, as well as in the

upstream and downstream segments of the cremaster arteriole. For each of the 3 locations, the main trend in the median velocity was an increase (up to \approx 2-fold) followed by a slower decrease (Figure 2D through 2F). For all clotting events, the velocities were positive, even for those with zero above-clot lumen (full-diameter clots).

Injury Length Determines the Amount of Platelet and Fibrin Deposition

Maximum platelet and fibrin accumulation reflects the maximum capacity of a clot to block blood flow. Because we were interested in this capacity, we used maximum fluorescence (ie, the maximum value of the bulk-fluorescence time course), calculated for individual thrombi, as the integral measure of bulk accumulation for platelets and fibrin at the injury site. Maximum platelet fluorescence on the logarithmic scale did not show a significant correlation with the arteriole diameter at the injury site (Figure II in the [Data Supplement](#)). Thus, we considered the following 3 variables as potential predictors for maximum platelet fluorescence: injury length and the maximum up- and downstream-diameter fold change. Using stepwise regression, we obtained a reduced regression equation, which we then extrapolated to the case of no upstream and no downstream deformation (by setting maximum diameter fold change to one). This yielded a regression equation with only one predictor—the injury length, which captured the data ($R^2=0.43$; Figure 3A). A separate fit of a single-variable regression model to the data produced an almost identical regression line, corroborating that the measured upstream and downstream deformations indeed played a minimal role in bulk clot accumulation ($R^2=0.35$; Figure 3A).

The generated linear model suggested that linear-scale maximum platelet fluorescence could be captured by an exponential dependence on injury length. This dependence captured the data, albeit with a higher level of statistical variability (ie, a smaller $R^2=0.19$; Figure 3B). Consistent with the stepwise-regression analysis, there was no correlation between the arteriole deformations and linear-scale maximum platelet fluorescence (Figure III in the [Data Supplement](#)).

We next applied this analysis strategy to the fibrin fluorescence data. This analysis was more straightforward because stepwise regression automatically reduced the initial, multivariable regression model to a univariate model depending only on injury length (Figure 3C). Interestingly, the exponential model (Figure 3D) fit the data with a slightly higher $R^2=0.45$ than that for the corresponding log-scale model ($R^2=0.42$, Figure 3C; this effect was even more pronounced for the fibrin area under the curve mentioned below).

We applied the same analysis strategy to the platelet and fibrin area under the curve, which is another frequently used quantitative parameter of time-course

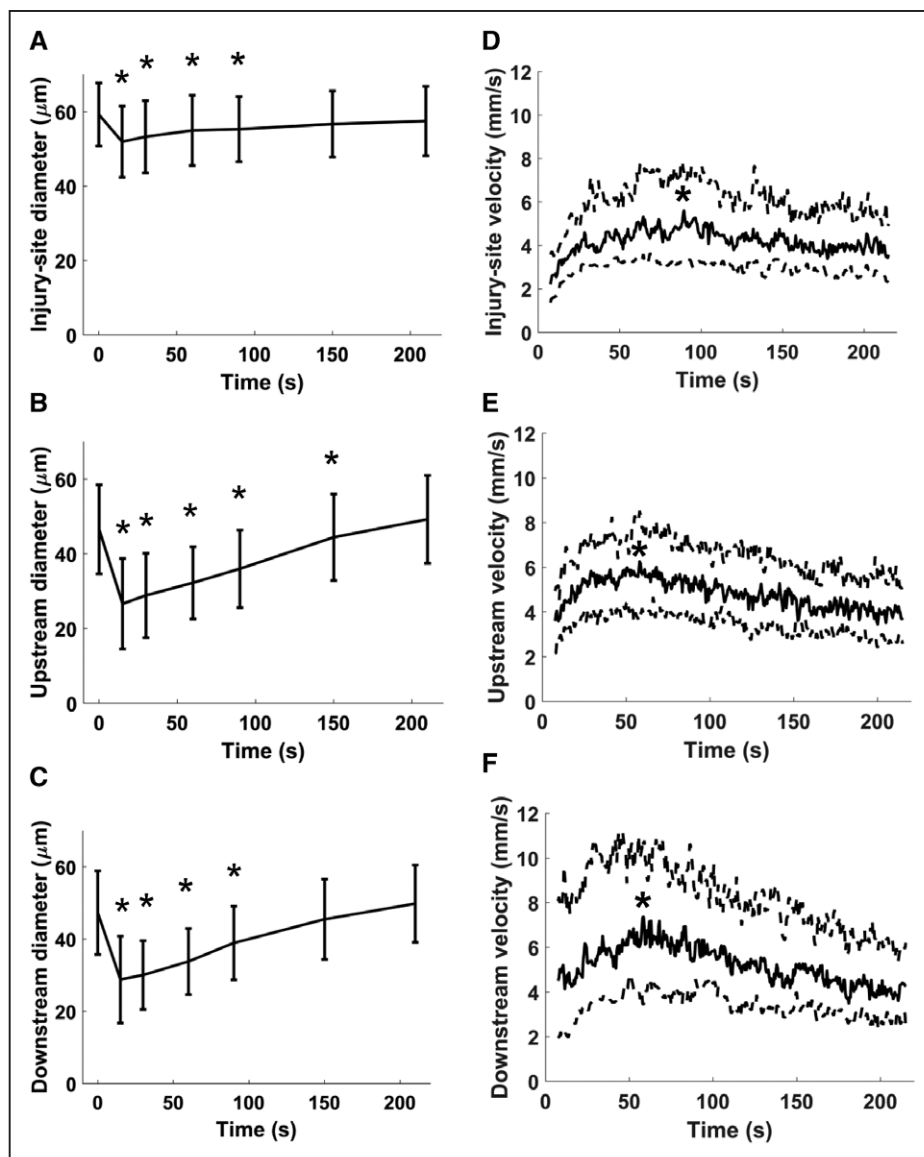


Figure 2. Arteriole deformation and blood-flow dynamics.

In each subplot, N=59. **A, B, and C,** Cremaster-arteriole diameters measured at the injury site, upstream of it (130 μm), and downstream of it (130 μm), respectively. The diameters were measured at 0, 15, 30, 60, 90, 180, and 210 s. The data points and error bars represent the means and 1 SD, respectively; the lines are shown to enhance visual presentation of the trends. The asterisks show statistically significant differences ($P < 0.0033$; Bonferroni-corrected with correction factor 6) between the diameter at the indicated time and that at time 0. **D, E, and F,** Flow-velocity dynamics measured at the injury site, upstream of it, and downstream of it, respectively. Solid and dashed lines show the medians and interquartile distances, respectively. The asterisks designate peak median. The increase in the injury-site, upstream, and downstream velocity (median velocity at the initial time vs peak median) was significant ($P = 6.3 \times 10^{-7}$, 1.0×10^{-8} , and 6.0×10^{-3} , respectively).

data. The results were similar to those for maximum fluorescence (Figure IV in the [Data Supplement](#); Figure 3E and 3F).

Injury Length and Arteriole Diameter Determine Platelet Clot Height, but Time to Maximum Fluorescence Is Independent of Injury Length

The logarithmic-scale functional relationships for the platelet bulk-accumulation parameters suggested that such logarithmic quantities could be quantitatively linked

to clot height. Indeed, univariate linear regression identified a strong functional relationship of this kind (Figure 4A and 4B). These results, together with the linear relationship between the bulk-accumulation logarithms and injury length, suggested a possible linear association between injury length and clot height. Naturally, we expected that the arteriole diameter would also affect clot height, which prompted us to perform a 2-variable linear regression analysis. It identified a significant increasing relationship between clot height and injury length (Figure 4C and 4D).

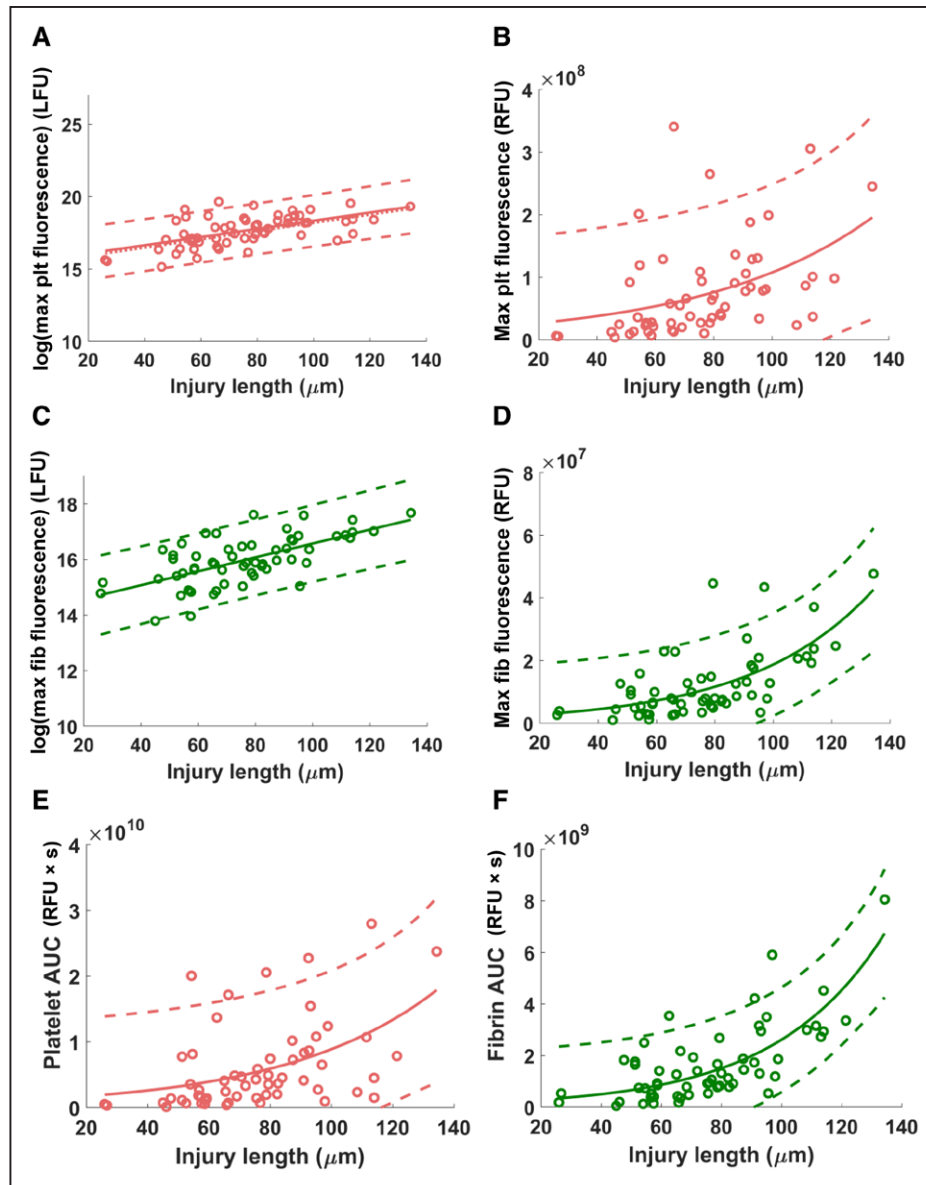


Figure 3. Bulk platelet and fibrin accumulation as a function of injury length.

In each subplot, the circles represent individual clotting events ($N=59$). The solid and dashed lines represent the univariate regression lines and the corresponding 95% prediction intervals, respectively. **A**, Maximum of the platelet bulk-fluorescence time course (logarithmic fluorescence units [LFU]). The dotted line represents the reduced regression equation (ie, the result of stepwise regression) with maximum deformation fold change set to 1. Regression analysis: $R^2=0.43$, $P=1.0 \times 10^{-5}$ (stepwise); $R^2=0.35$, $P=6.7 \times 10^{-7}$ (univariate). **B**, Maximum of the platelet bulk-fluorescence time course (raw fluorescence units [RFUs]). Regression analysis: $R^2=0.19$. **C**, Maximum of the fibrin bulk-fluorescence time course (LFU). Regression analysis: $R^2=0.42$, $P=3.4 \times 10^{-8}$. **D**, Maximum of the fibrin bulk-fluorescence time course (RFU). Regression analysis: $R^2=0.45$. **E**, Platelet bulk-fluorescence time-course area under the curve (AUC). Regression analysis: $R^2=0.21$. **F**, Fibrin bulk-fluorescence time-course AUC. Regression analysis: $R^2=0.57$.

Taken together, our findings indicated that injury length was a strong determinant of the amount of platelet and fibrin accumulation. In contrast, the times to maximum bulk fluorescence for the individual platelet and fibrin bulk-fluorescence time courses did not show a well-pronounced association with injury size (Figure 4E and 4F). For a small fraction of the clots, the maximum levels were achieved at the very beginning (Figure 4E and 4F), reflecting the (transient) platelet and fibrin accumulation that was already occurring when the time-course

measurements began (ie, within ≈ 1 seconds from the time of injury).

After Clot Growth Onset, Injury-Site flow Velocity Is Negatively Correlated With Arteriole Diameter and With the Above-Clot Lumen Size

Centerline flow-velocity is expected to be proportional to the arteriole diameter in unperturbed microvascular beds (see Equations I through IV in the [Data Supplement](#)).

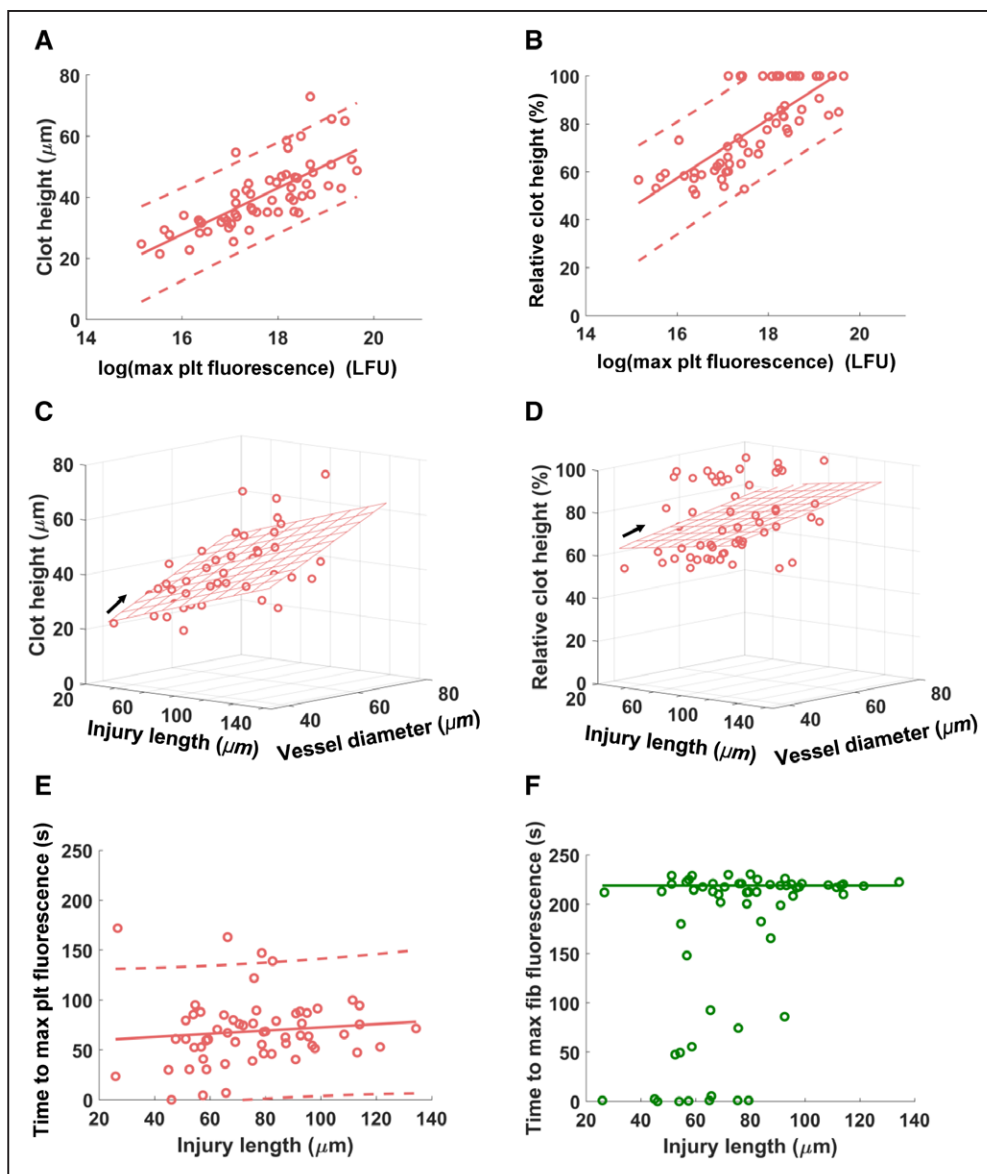


Figure 4. Dependence of the platelet-clot height and time to maximum fluorescence on injury length.

In each subplot, the circles represent individual clotting events ($N=59$). LFU, logarithmic fluorescence units (log of RFU). **A**, **B**, and **E**, The solid and dashed lines represent univariate regression lines and the corresponding 95% prediction intervals, respectively. **A**, The height of the platelet clot measured at its maximum value. Regression analysis: $R^2=0.55$, $P=1.4 \times 10^{-11}$. **B**, Relative clot height, defined as the percent-ratio of the platelet-clot height (measured at the time of the clot's maximum extent) to the arteriole diameter at the site of injury (measured at the same time). Regression analysis: $R^2=0.58$, $P=3.0 \times 10^{-12}$. **C**, Clot height as a function of injury length and arteriole diameter at the injury site measured when the platelet clot reached its maximum height. Bivariate linear regression (surface): $R^2=0.45$, $P=6.5 \times 10^{-8}$. Black arrow indicates the slope of the dependency of clot height on injury length. **D**, Relative clot height as a function of injury length and arteriole diameter at the injury site measured at the time of the clot's maximum extent. Bivariate linear regression (surface): $R^2=0.23$, $P=6.3 \times 10^{-4}$. Black arrow, as in **(C)**. **E**, Time to maximum platelet bulk fluorescence as a function of injury length. Regression analysis: $R^2=0.01$, $P=0.41$. **F**, Time to maximum fibrin bulk fluorescence as a function of injury length. The time-to-maximum values were binned into 30 equal-sized bins, and the center of the bin with the largest number of time-to-maximum values is indicated by the solid line.

To test this relationship in our laser-injury model, we performed univariate linear regression analysis for the injury-site velocity values measured at an early time point (9 seconds). The analysis identified a pronounced positive association (Figure 5A), which persisted when we repeated this analysis for other early time points. In contrast, when we chose a significantly later time point, the pattern dramatically changed. Specifically, for

injury-site velocity at 90 seconds (chosen as a characteristic time for a pronounced thrombus [Figure 1D]), the linear relationship became negative (Figure 5B)—a trend that persisted for velocity values measured at other (similar) times.

Because the arteriole constriction at the injury site was quick, small, and transient (Figure 2A), and because substantial clots were present by as late as 70 seconds

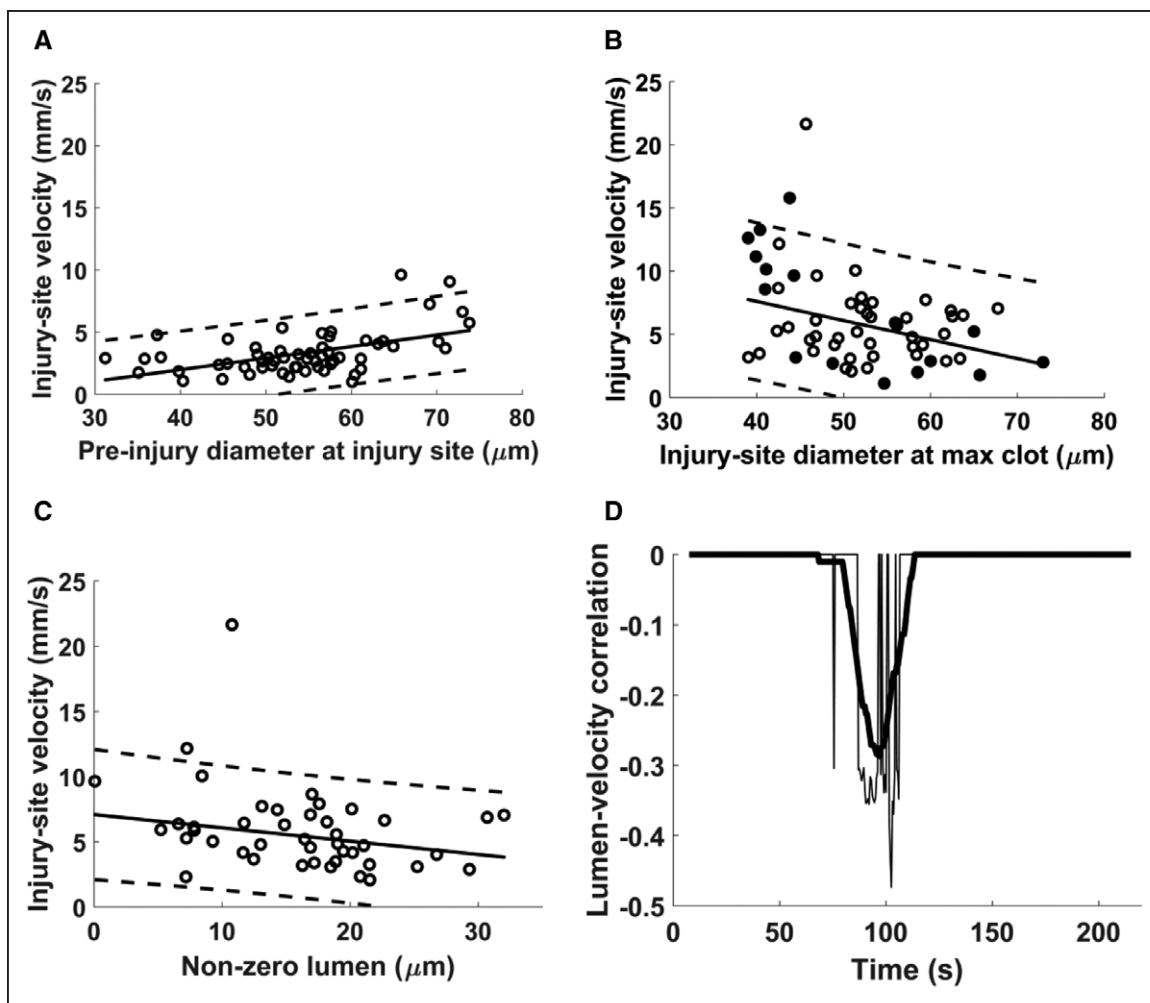


Figure 5. Flow velocity in the vicinity of the injury site.

A–C, The circles represent individual clotting events; the solid and dashed lines represent univariate regression lines and the corresponding 95% prediction intervals, respectively. **A,** Dependence of the velocity measured at 9 s on the preinjury arteriole diameter measured at the injury site ($N=59$). Regression analysis: $R^2=0.26$, $P=3.3\times 10^{-5}$. **B,** Dependence of the velocity measured at 90 s on the arteriole diameter measured at the injury site at the time of the clot's maximum extent ($N=59$). The black circles mark the 16 clots with zero above-clot lumen. The regression ($R^2=0.16$, $P=0.002$) was performed with the robustopt (robust regression) option activated to decrease the influence of apparent outliers. **C,** Dependence of the velocity measured at 90 s on the size of the arteriole above-clot lumen (Figure 1C) measured at the injury site at the time of the clot's maximum extent. The analysis was performed only for the clots with nonzero lumen ($N=43$). The regression ($R^2=0.12$, $P=0.02$) was performed with the robustopt option activated. **D,** Correlation coefficients between the velocity measured at the indicated times (x -axis) and the size of the above-clot lumen measured at the injury site at the time of the clot's maximum extent. The thin lines correspond to statistically significant ($P<0.05$) correlation coefficients, and the thick line is a result of moving-average smoothing of the thin line. The analysis was performed only for the clots with nonzero lumen ($N=43$).

to 90 seconds (Figure 1D), the detected change in the velocity pattern could be attributed directly to the presence of the clot. Interestingly, the pattern was driven by the 16 thrombi with a zero above-clot lumen (full-diameter thrombi), because this pattern was reflected by the regression calculated for this group of thrombi ($R^2=0.49$, $P=0.003$), whereas the regression calculated for the 43 partial-diameter thrombi ($R^2=0.04$, $P=0.18$) returned a flat line (Figure V in the [Data Supplement](#)).

These findings suggested that, for partial-diameter thrombi, a more informative velocity-associated parameter could be the size of the above-clot lumen (rather than arteriole diameter). We probed this association using

linear regression for the 43 partial-diameter (ie, non-zero-lumen) thrombi (Figure 5C). The analysis showed that, consistent with our expectations, the velocity at 90 seconds was increased for small lumens (Figure 5C). We then tested this pattern for the velocities measured at other times. To this end, we calculated correlation coefficients between the lumen size and the velocities measured at different times and set the nonsignificant correlation coefficients to zero. As expected, the resulting temporal dependence demonstrated a persistent negative correlation between the lumen and the velocity (Figure 5D). That correlation was the strongest at ≈ 100 seconds, which corresponded to the time frame

of maximum median platelet deposition at the injury site (Figure 1D). These results suggested that the detected increase in the injury-site flow velocity was largely due to the growth of the clot.

Upstream Flow Velocity Is Defined by Arteriole Deformation and a Time Delay and Determines Downstream Velocity

To investigate the relationship between the upstream flow velocity and the upstream arteriole diameter, we first calculated, for each clotting event, the correlation coefficient between the time-dependent diameter measurements and the velocity values measured at the

corresponding times. For 47 out of 59 clotting events, the correlation coefficients were negative, indicating a decreasing functional relationship (Figure 6A). Yet, 12 of the coefficients was positive, prompting further analysis. We then used all 59 clots to calculate the velocity-diameter correlation coefficient for these quantities measured at 15 seconds (ie, when the measured arteriole constriction was maximal [Figure 2B]). The results indicated no significant correlation (Figure 6B). We then hypothesized that a stronger association could be detected between the diameter measured at 15 seconds and the velocity measured at 50 seconds, that is, around the time when median upstream velocity reached its peak value (Figure 2E). Regression analysis of these 2 quantities

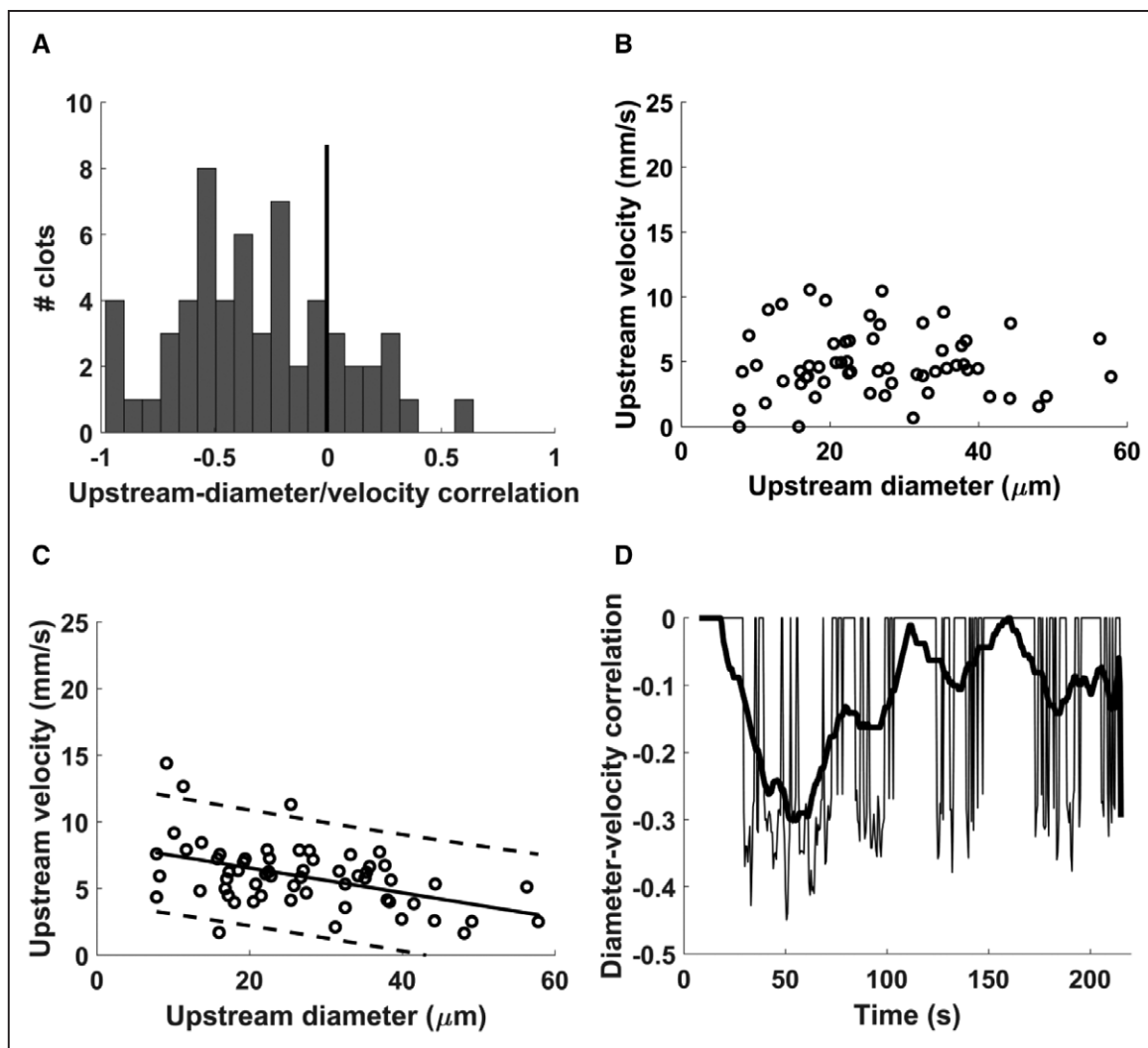


Figure 6. Flow velocity upstream of the injury site.

In each subplot, $N=59$. **A**, histogram of the correlation coefficients between the upstream-diameter measurements (at the times indicated in Figure 2A through 2C) and the corresponding upstream-velocity measurements for each clotting event. Six of the coefficients were significant. The vertical line separates positive and negative correlation coefficients. In **(B)** and **(C)**, the circles represent individual clotting events. The solid and dashed lines represent univariate regression lines and the corresponding 95% prediction intervals, respectively. **B**, Dependence of the upstream velocity measured at 15 s on the upstream diameter measured at 15 s. Correlation analysis: $\rho=0.04$, $P=0.76$. **C**, Dependence of the upstream velocity measured at 50 s on the upstream diameter measured at 15 s. Regression analysis: $R^2=0.22$, $P=1.8 \times 10^{-4}$. **D**, Correlation coefficients between the upstream velocity measured at the indicated times (x -axis) and the upstream diameter at 15 s. The thin lines correspond to statistically significant ($P<0.05$) correlation coefficients, and the thick line is a result of moving-average smoothing of the thin line.

demonstrated a pronounced negative association (Figure 6C). We repeated this analysis (similarly to Figure 5D), calculating the correlation coefficients for the diameter at 15 seconds and upstream velocities at different time points. The results indicated consistent negative correlations, with the strongest negative correlations at times near 50 seconds (Figure 6D), when the velocity was the highest (Figure 2E).

These results suggested that the fast constriction of the arteriole upstream of the injury caused a delayed increase in the upstream velocity. The correlation coefficients in Figure 6A were calculated without taking the delay into account, which may explain why some of them were positive. Because the arteriole diameters up- and downstream of the injury were very similar (Figure 2B and 2C), we expected—based on the law of mass conservation—that the up- and downstream velocity profiles would be similar as well, which was confirmed by our data (Figure 2E and 2F).

DISCUSSION

Here, we investigated the interrelations between injury severity, clot formation, cremaster-arteriole deformation, and blood flow in a mouse model of laser-induced injury. In our experiments, bulk platelet and fibrin deposition demonstrated nonlinear dependencies on the injury length. The height of the platelet clot and its relative height (with respect to arteriole diameter) were determined by injury length and the arteriole diameter. Clot growth was linked to a change in the flow-velocity pattern in the injured vessel, which differed from that for unperturbed flow. In this altered pattern, increased injury-site velocity corresponded to a reduced size of the above-clot lumen in the arteriole. Upstream and downstream velocity synchronously increased and then decreased, which correlated with transient arteriole constriction.

The constriction of arterioles is controlled by their muscular walls. The consistent pattern of the detected constrictions (namely, similarly pronounced upstream and downstream, much less pronounced at the injury site) suggests tight regulation (Figure 2A through 2C). The speed of the constriction reaction (seconds after injury) suggests that its main mechanism involves either neural regulation³³ or the spontaneous ability of the muscle to constrict in response to injury.³⁴

The similarity of injury-dependent regulation patterns between platelets and fibrin (Figure 3) is intriguing, given their intrinsic functional differences. Another intriguing result is the contrast between exponential bulk-clot accumulation and the linear relationship between platelet-clot height and injury length (and also the arteriole diameter, Figure 4C and 4D). The link between clot height and injury length serves as evidence that increased injury severity can result in an increased capacity for blood-vessel obstruction and, possibly, thrombotic complications.

The effects of blood flow on clot growth *in vivo* have been extensively studied.^{2,35} Here, we focused on the effects of clot growth on blood flow. Microvascular research suggests that, in general, blood-flow velocity is positively correlated with vessel diameter.³⁶ More specifically, based on considerations of mechanical energy minimization, volumetric flow rate in arterioles is expected to be proportional to diameter cubed,^{37,38} leading to the positive linear relationship between the diameter and centerline flow velocity outlined in the Equations I through IV in the [Data Supplement](#). Our results for the blood flow measured before clot formation were consistent with this pattern (Figure 5A). Yet, the picture for both clot formation (Figure 5B and 5C) and arteriole constriction (Figure 6C) was directly opposite, with a negative relationship between the velocity and the passage size. This suggests that clot formation and arteriole constriction were associated with a dynamic change in the physiology of the system, with a flow-velocity increase (Figure 2D through 2F) reminiscent of reactive hyperemia³⁹ but without full arterial occlusion. This physiological change may be explained by the action of microvascular networks, which can actively regulate and redistribute blood flow.^{24,25} The resultant negative diameter-velocity relationship may contribute to the flow-mediated effects on the clot—some of which, such as shear-induced platelet activation, require increased flow velocity at clot surface.^{1,28}

In a blood-vessel segment, the pressure drop, flow resistance, and volumetric flow rate are the 3 main physical quantities characterizing the fluid mechanics within the vessel. These quantities are coupled together through a relationship wherein the pressure drop is equal to the product of flow resistance and flow rate. Our analysis has focused primarily on the associations between flow velocity and arteriole diameter, because centerline velocity is directly proportional to volumetric flow rate,⁴⁰ and arteriole diameter is inversely related to flow resistance (for Poiseuille flows, the resistance is inversely proportional to the diameter raised to the power four⁴¹). Whereas it is natural to expect that the arterial-segment resistance (modulated by the growing clot) will affect the velocity of the flow through the segment, this relationship is complicated by the potential influence of the microvascular bed surrounding the arteriole segment. Indeed, laser injury might lead to a complex redistribution of pressure gradients, resistances, and flows in the local arteriolar network. This possibility complicates causal analysis of the mechanistic factors that determine the velocity changes detected in our experiments, and provides a justification for our data-driven analysis.

Our study has limitations. First, there are general limitations associated with our thrombosis model, including the artificial clotting trigger (laser light). While each of the existing experimental models of thrombosis has its limitations,⁴² our model has been extensively studied¹¹ and could therefore yield reliable measurements directly

comparable with the results of other investigations. At the same time, our methods and results can be tested using other injury models in other mouse blood vessels, as well as in genetically modified or diseased mice. The second limitation is associated with our data-driven approach centered on correlation and regression analysis of imaging data. This methodology could not provide insights into the physiological mechanisms behind the detected arteriole constriction or a detailed explanation of the transition from a positive diameter-velocity relationship to a negative one. Moreover, the potential influence of the surrounding microvascular network on the flow in the arteriole segment of interest could not be quantified, which complicated causal interpretation of the observed velocity changes. Yet, the diverse mechanistic questions raised by the present work would require very different research methodologies and would be unfeasible to unite in one study. The strength of the identified statistical dependencies reflects the dominance of the factors included in the analysis in the presence of possible confounders. The third potential limitation is the presence of considerable variability in our platelet and fibrin bulk-accumulation data. Whereas some of the variability could be attributed to variations in injury length (Figures 3 and 4), and while platelet response is known to be intrinsically heterogeneous,¹² the noise may have blurred certain functional relationships between variables of interest. In addition, injury depth could have influenced clot growth but was not investigated in our study. Further research is needed to more fully explain the variability of thrombus formation in vivo and to increase the robustness of the detected quantitative patterns.

The quantitative relationships established in this study can be tested not only for diverse pathological conditions but also in the presence of therapeutic interventions aimed to control thrombus development. This may allow us to better understand how the strength and dosage of antithrombotic agents can be fine-tuned to achieve the desired blood-flow control without shifting the hemostatic balance toward bleeding. Moreover, the established quantitative patterns can facilitate the calibration and validation of computational models of clot formation in vivo, which would improve their accuracy and practical utility.

ARTICLE INFORMATION

Received March 12, 2020; accepted June 11, 2020.

Affiliations

From the DoD Biotechnology High Performance Computing Software Applications Institute, Telemedicine and Advanced Technology Research Center, US Army Medical Research and Development Command, Ft. Detrick, MD (A.Y.M., V.G., A.K., D.S.H., G.U., J.R.); The Henry M. Jackson Foundation for the Advancement of Military Medicine, Inc, Bethesda, MD (A.Y.M., V.G., A.K., D.S.H., G.U.); and Division of Hemostasis and Thrombosis, Department of Medicine, Beth Israel Deaconess Medical Center, Harvard Medical School, Boston, MA (G.M.-S., S.P.G., R.F.)

Sources of Funding

This work was supported by the US Army Medical Research and Development Command, Ft. Detrick, MD.

Disclosures

R. Flaumenhaft is a consultant for Platelet Diagnostics. The opinions and assertions contained herein are the private views of the authors and are not to be construed as official or as reflecting the views of the US Army, the US Department of Defense, or The Henry M. Jackson Foundation for the Advancement of Military Medicine, Inc. This article has been approved for public release with unlimited distribution. The other authors report no conflicts.

REFERENCES

- Jackson SP. Arterial thrombosis—insidious, unpredictable and deadly. *Nat Med*. 2011;17:1423–1436. doi: 10.1038/nm.2515
- Jackson SP, Nesbitt WS, Westein E. Dynamics of platelet thrombus formation. *J Thromb Haemost*. 2009;7(suppl 1):17–20. doi: 10.1111/j.1538-7836.2009.03401.x
- Ivanciu L, Stalker T.J. Spatiotemporal regulation of coagulation and platelet activation during the hemostatic response in vivo. *J Thromb Haemost*. 2015;13:1949–1959. doi: 10.1111/jth.13145
- Govindarajan V, Zhu S, Li R, Lu Y, Diamond SL, Reifman J, Mitrophanov AY. Impact of tissue factor localization on blood clot structure and resistance under venous shear. *Biophys J*. 2018;114:978–991. doi: 10.1016/j.bpj.2017.12.034
- Mitrophanov AY, Govindarajan V, Zhu S, Li R, Lu Y, Diamond SL, Reifman J. Microfluidic and computational study of structural properties and resistance to flow of blood clots under arterial shear. *Biomech Model Mechanobiol*. 2019;18:1461–1474. doi: 10.1007/s10237-019-01154-0
- Okorie UM, Denney WS, Chatterjee MS, Neeves KB, Diamond SL. Determination of surface tissue factor thresholds that trigger coagulation at venous and arterial shear rates: amplification of 100 fM circulating tissue factor requires flow. *Blood*. 2008;111:3507–3513. doi: 10.1182/blood-2007-08-106229
- Shen F, Kastrop CJ, Liu Y, Ismagilov RF. Threshold response of initiation of blood coagulation by tissue factor in patterned microfluidic capillaries is controlled by shear rate. *Arterioscler Thromb Vasc Biol*. 2008;28:2035–2041. doi: 10.1161/ATVBAHA.108.173930
- Zhu S, Tomaiuolo M, Diamond SL. Minimum wound size for clotting: flowing blood coagulates on a single collagen fiber presenting tissue factor and von Willebrand factor. *Integr Biol (Camb)*. 2016;8:813–820. doi: 10.1039/c6ib00077k
- Mitrophanov AY, Wolberg AS, Reifman J. Kinetic model facilitates analysis of fibrin generation and its modulation by clotting factors: implications for hemostasis-enhancing therapies. *Mol Biosyst*. 2014;10:2347–2357. doi: 10.1039/c4mb00263f
- Chatterjee MS, Denney WS, Jing H, Diamond SL. Systems biology of coagulation initiation: Kinetics of thrombin generation in resting and activated human blood. *PLOS Comput Biol*. 2010;6:e1000950. doi: 10.1371/journal.pcbi.1000950
- Bellido-Martín L, Chen V, Jusuja R, Furie B, Furie BC. Imaging fibrin formation and platelet and endothelial cell activation in vivo. *Thromb Haemost*. 2011;105:776–782. doi: 10.1160/TH10-12-0771
- Munnix IC, Cosemans JM, Auger JM, Heemskerk JW. Platelet response heterogeneity in thrombus formation. *Thromb Haemost*. 2009;102:1149–1156. doi: 10.1160/TH09-05-0289
- Falati S, Gross P, Merrill-Skoloff G, Furie BC, Furie B. Real-time *in vivo* imaging of platelets, tissue factor and fibrin during arterial thrombus formation in the mouse. *Nat Med*. 2002;8:1175–1181. doi: 10.1038/nm782
- Sumi T, Yamashita A, Matsuda S, Goto S, Nishihira K, Furukoji E, Sugimura H, Kawahara H, Imamura T, Kitamura K, et al. Disturbed blood flow induces erosive injury to smooth muscle cell-rich neointima and promotes thrombus formation in rabbit femoral arteries. *J Thromb Haemost*. 2010;8:1394–1402. doi: 10.1111/j.1538-7836.2010.03843.x
- Hechler B, Nonne C, Eckly A, Magnenat S, Rinckel JY, Denis CV, Freund M, Cazenave JP, Lanza F, Gachet C. Arterial thrombosis: relevance of a model with two levels of severity assessed by histologic, ultrastructural and functional characterization. *J Thromb Haemost*. 2010;8:173–184. doi: 10.1111/j.1538-7836.2009.03666.x
- Nonne C, Lenain N, Hechler B, Mangin P, Cazenave JP, Gachet C, Lanza F. Importance of platelet phospholipase Cgamma2 signaling in arterial thrombosis as a function of lesion severity. *Arterioscler Thromb Vasc Biol*. 2005;25:1293–1298. doi: 10.1161/01.ATV.0000163184.02484.69

17. Kadri OE, Chandran VD, Surblyte M, Voronov RS. *In vivo* measurement of blood clot mechanics from computational fluid dynamics based on intravital microscopy images. *Comput Biol Med*. 2019;106:1–11. doi: 10.1016/j.combiomed.2019.01.001
18. Govindarajan V, Rakesh V, Reifman J, Mitrophanov AY. Computational study of thrombus formation and clotting factor effects under venous flow conditions. *Biophys J*. 2016;110:1869–1885. doi: 10.1016/j.bpj.2016.03.010
19. Colace TV, Muthard RW, Diamond SL. Thrombus growth and embolism on tissue factor-bearing collagen surfaces under flow: role of thrombin with and without fibrin. *Arterioscler Thromb Vasc Biol*. 2012;32:1466–1476. doi: 10.1161/ATVBAHA.112.249789
20. Lockyer S, Kambayashi J. Demonstration of flow and platelet dependency in a ferric chloride-induced model of thrombosis. *J Cardiovasc Pharmacol*. 1999;33:718–725. doi: 10.1097/00005344-199905000-00007
21. Quaknine-Orlando B, Samama CM, Riou B, Bonnin P, Guillosson JJ, Beaumont JL, Coriat P. Role of the hematocrit in a rabbit model of arterial thrombosis and bleeding. *Anesthesiology*. 1999;90:1454–1461. doi: 10.1097/00000542-199905000-00031
22. Ungersböck K, Heimann A, Kempfski O. Cerebral blood flow alterations in a rat model of cerebral sinus thrombosis. *Stroke*. 1993;24:563–9; discussion 569. doi: 10.1161/01.str.24.4.563
23. Zaman AG, Osende JL, Chesebro JH, Fuster V, Padurean A, Gallo R, Worthley SG, Helft G, Rodriguez OX, Fallon JT, et al. *In vivo* dynamic real-time monitoring and quantification of platelet-thrombus formation: use of a local isotope detector. *Arterioscler Thromb Vasc Biol*. 2000;20:860–865. doi: 10.1161/01.atv.20.3.860
24. Secomb TW. Theoretical models for regulation of blood flow. *Microcirculation*. 2008;15:765–775. doi: 10.1080/10739680802350112
25. Secomb TW, Pries AR. The microcirculation: physiology at the mesoscale. *J Physiol*. 2011;589(pt 5):1047–1052. doi: 10.1113/jphysiol.2010.201541
26. Leiderman K, Fogelson AL. Grow with the flow: a spatial-temporal model of platelet deposition and blood coagulation under flow. *Math Med Biol*. 2011;28:47–84. doi: 10.1093/imammb/dqq005
27. Tomaiuolo M, Stalker TJ, Welsh JD, Diamond SL, Sinno T, Brass LF. A systems approach to hemostasis: 2. Computational analysis of molecular transport in the thrombus microenvironment. *Blood*. 2014;124:1816–1823. doi: 10.1182/blood-2014-01-550343
28. Nesbitt WS, Westein E, Tovar-Lopez FJ, Tolouei E, Mitchell A, Fu J, Carberry J, Fouras A, Jackson SP. A shear gradient-dependent platelet aggregation mechanism drives thrombus formation. *Nat Med*. 2009;15:665–673. doi: 10.1038/nm.1955
29. Higgins SJ, De Ceunynck K, Kellum JA, Chen X, Gu X, Chaudhry SA, Schulman S, Libermann TA, Lu S, Shapiro NI, et al. Tie2 protects the vasculature against thrombus formation in systemic inflammation. *J Clin Invest*. 2018;128:1471–1484. doi: 10.1172/JCI97488
30. Glantz SA. Primer of biostatistics. *Yale J Biol Med*. 2012;85:432–433.
31. Jarque CM, Bera AK. A test for normality of observations and regression residuals. *Internat Statist Rev*. 1987;55:163–172.
32. Mitrophanov AY, Szlam F, Sniecinski RM, Levy JH, Reifman J. Controlled multifactorial coagulopathy: effects of dilution, hypothermia, and acidosis on thrombin generation *In Vitro*. *Anesth Analg*. 2020;130:1063–1076. doi: 10.1213/ANE.00000000000004479
33. McGillivray-Anderson KM, Faber JE. Effect of acidosis on contraction of microvascular smooth muscle by alpha 1- and alpha 2-adrenoceptors. Implications for neural and metabolic regulation. *Circ Res*. 1990;66:1643–1657. doi: 10.1161/01.res.66.6.1643
34. Lagaud G, Gaudreault N, Moore ED, Van Breemen C, Laher I. Pressure-dependent myogenic constriction of cerebral arteries occurs independently of voltage-dependent activation. *Am J Physiol Heart Circ Physiol*. 2002;283:H2187–H2195. doi: 10.1152/ajpheart.00554.2002
35. Cosemans JM, Angelillo-Scherrer A, Mattheij NJ, Heemskerk JW. The effects of arterial flow on platelet activation, thrombus growth, and stabilization. *Cardiovasc Res*. 2013;99:342–352. doi: 10.1093/cvr/cvt110
36. Pries AR, Secomb TW, Gaehtgens P. Biophysical aspects of blood flow in the microvasculature. *Cardiovasc Res*. 1996;32:654–667.
37. Mayrovitz HN, Roy J. Microvascular blood flow: evidence indicating a cubic dependence on arteriolar diameter. *Am J Physiol*. 1983;245:H1031–H1038. doi: 10.1152/ajpheart.1983.245.6.H1031
38. Zamir M. Shear forces and blood vessel radii in the cardiovascular system. *J Gen Physiol*. 1977;69:449–461. doi: 10.1085/jgp.69.4.449
39. Olsson RA. Myocardial reactive hyperemia. *Circ Res*. 1975;37:263–270. doi: 10.1161/01.res.37.3.263
40. Goldsmith HL, Turitto VT. Rheological aspects of thrombosis and haemostasis: basic principles and applications. ICTH-report–subcommittee on rheology of the international committee on thrombosis and haemostasis. *Thromb Haemost*. 1986;55:415–435.
41. Secomb TW. Blood flow in the microcirculation. *Ann Rev Fluid Mech*. 2017;49:443–461.
42. Jagadeeswaran P, Cooley BC, Gross PL, Mackman N. Animal models of thrombosis from zebrafish to nonhuman primates: use in the elucidation of new pathologic pathways and the development of antithrombotic drugs. *Circ Res*. 2016;118:1363–1379. doi: 10.1161/CIRCRESAHA.115.306823